

ARE LARGE X-RAY CLUSTERS AT THERMAL EQUILIBRIUM ?

JEAN-PIERRE CHIÈZE

CEA, DSM/DAPNIA/Service d’Astrophysique, CE SACLAY, F-91191 Gif-sur-Yvette,
France

JEAN-MICHEL ALIMÌ

Laboratoire d’Astrophysique Extragalactique et de Cosmologie, CNRS URA 173,
Observatoire de Paris-Meudon, 92195 Meudon, France

ROMAIN TEYSSIER

CEA, DSM/DAPNIA/Service d’Astrophysique, CE SACLAY, F-91191 Gif-sur-Yvette,
France

ABSTRACT

We simulate the formation of a large X-ray cluster using a fully 3D hydrodynamical code coupled to a Particle–Mesh scheme which models the dark matter component. We focus on a possible decoupling between electrons and ions temperatures. We then solve the energy transfer equations between electrons, ions and neutrals without assuming thermal equilibrium between the three gases ($T_e \neq T_i \neq T_n$). We solve self-consistently the chemical equations for an hydrogen/helium primordial plasma without assuming ionization–recombination equilibrium. We find that the electron temperature differs from the true dynamical temperature by 20% at the Virial radius of our simulated cluster. This could lead marginally to an underestimate of the total mass in the outer regions of large X-ray clusters.

Subject headings: cosmology: theory – hydrodynamics – X-rays: clusters –
methods: numerical

1. INTRODUCTION

Large X-ray clusters are well defined cosmological objects which can provide useful constraints on currently discussed structure formation theories. It is believed that they are composed mainly of dark matter and X-ray emitting gas. The physical conditions of the hot gas are rather extreme. Common values for the electrons density range from 10^{-1} cm^{-3}

in the core to 10^{-5} cm^{-3} in the outer regions. The electrons temperature is about 10 keV, up to 15 keV for A2163, the hottest cluster known so far (Arnaud et al. 1992).

Recently, Markevitch et al. (1996) studied the electrons temperature profile of A2163 using different X-ray experiments. They measured $T_e \simeq 4 \text{ keV}$ at a radius corresponding roughly to the Virial radius of the cluster ($r_{200} \simeq 2.4 \text{ Mpc h}^{-1}$). Using the well known hydrostatic equilibrium equation in order to derive the total mass distribution, they conclude that the total mass distribution is significantly steeper than the X-ray gas distribution. But, as shown by Schindler & Muller (1993) and Evrard, Metzler & Navarro (1996), the hydrostatic equilibrium assumption is unlikely to be true in the low density regions. Moreover, at that radius, the electron density is supposed to be roughly a few 10^{-5} cm^{-3} , and the time-scale for electrons to reach thermodynamical equilibrium with ions is then about 4 Gyr, comparable to the merger time-scale (Markevitch et al. 1996). Therefore, one can ask the following question: in the outer region of A2163 and more generally in any large X-ray cluster, is $T_e = T_i$? If $T_e \neq T_i$, this could result in additional errors in the mass estimate due to a departure from thermodynamical equilibrium between ions and electrons.

In Teyssier, Chièze & Alimi (1997), as a first approach to this problem, we studied the collapse of a planar density perturbation, usually called a Zel’dovich pancake, of comoving wavelength $L = 16 \text{ Mpc h}^{-1}$. This rather formal case enabled us to test with high resolution 1D simulations our hydrodynamical code which solves a set of collisional processes such as energy exchange, non-equilibrium chemistry, shock heating and electronic conduction. We showed that a large region of the pancake ($\simeq 1 \text{ Mpc h}^{-1}$) does not recover thermodynamical equilibrium. Only the central part of the pancake recovers within a few percent $T_e \simeq T_i$. The strongest departure from thermodynamical equilibrium was found near the shock front, where T_e is one order of magnitude lower than T_i .

For a real cluster, much higher densities and temperatures than for pancakes are expected in the high temperature, X-ray emitting gas. In this paper, we thus intend to make a quantitative study of the thermodynamical history of the gas during the hierarchical formation of a three-dimensional (3D) X-ray cluster embedded in a standard CDM cosmogony. We solve precisely the energy transfer equations between electrons, ions and neutrals, in order to confirm or infirm the thermodynamical equilibrium assumption.

To test the thermodynamical evolution of a realistic X-ray cluster, we have developed a 3D hydrodynamical code, called HYDREL (“HYDrodynamique Euler Lagrange”), coupled to a PM scheme which describes the dark matter component. In section 2 we describe the physical processes involved in the primordial collisional plasma, the numerical methods we use to simulate the formation of X-ray clusters. and the initial conditions we choose. In section 3 we present our results, showing that significant departure from thermodynamical

equilibrium can be obtained at a radius $r \simeq r_{200}$ ¹. We discuss the general properties of the simulated cluster, which has several average characteristics similar to those of the Coma cluster. Finally, in section 4, we discuss possible observational consequences of our work, such as an underestimation of the total mass in the outer regions of large X-ray clusters.

2. PHYSICAL AND NUMERICAL METHODS

In this paper, we intend to give a self-consistent description of the thermodynamical evolution of a cluster of galaxy embedded in an Einstein-de Sitter universe. We use the so-called “standard CDM cosmogony” with $\Omega = 1$, $\Omega_B = 0.1$ and $h = 0.5$. This scenario is one of the most typical example of the hierarchical clustering picture. We use the Bardeen et al. (1986) power spectrum to generate our initial Gaussian random field. In this section, we briefly recall the physical processes that we study here. We also present our numerical algorithm, namely the 3D hydrodynamical code HYDREL and we finally discuss the numerical parameters that we use for the specific realization presented here.

2.1. Physical Processes

The aim of this paper is to study the effect of several processes which we believe to be relevant in the primordial collisional plasma. We therefore focus on collisional processes and distinguish three thermodynamical species, namely electrons, ions and neutrals. Each specy is supposed to be individually at the local thermodynamical equilibrium (LTE), but we allow $T_e \neq T_i \neq T_n$, where the subscripts design electrons, ions and neutrals respectively. The LTE hypothesis is valid since the “isotropization time-scale” t_{iso} , which drives the distribution function of a given specy to a Maxwellian, is very small, even in the rather extreme conditions found in X-ray clusters. Indeed, from $n_e \simeq n_i = 10^{-5} \text{ cm}^{-3}$ and $T_e \simeq T_i = 10^7 \text{ K}$, we can deduce an estimation of $t_{iso} \simeq 10^5 \text{ yrs}$ for electrons and $t_{iso} \simeq 10^6 \text{ yrs}$ for ions (Spitzer 1962). On the other hand, we outlined in the introduction that the “equipartition time-scale” between electrons and ions was quite long in the outer regions ($t_{ei} \geq 10^9 \text{ yrs}$). We must therefore solve the energy transfer equations between the three thermodynamical species. Note that in the case of X-ray clusters, the neutral component is of weak relevance, since the medium is fully ionized. However, our code was designed for a more general use, and therefore we follow self-consistently all chemical species.

¹ r_{200} is the radius of the sphere centered on the cluster center and containing a mean over-density $\bar{\delta} = 200$

For electrons and protons, the internal energy transfer per unit volume and per unit time is due to Coulomb collisions and writes (Spitzer 1962)

$$\frac{\delta Q}{Dt} = -n_e n_p k (T_i - T_e) \left(\frac{4(2\pi)^{1/2} e^4 m_e^{1/2} \ln \Lambda_{ep}}{m_p (kT_{ei})^{3/2}} \right) \quad (1)$$

where T_{ei} is “the reduced temperature” of the two interacting particles and Λ_{ep} is the Coulomb logarithm. This formula can be applied to other ions with of course a modification due to their different atomic masses and charges (Spitzer 1962). We also compute the energy exchange rate between electrons and neutrals, using the classical “hard reflecting sphere” cross-section $\sigma_{en} \simeq 10^{-15} \text{ cm}^2$ (Draine & Katz 1986). The energy exchange between ions and neutrals which is due to the resonant charge transfer interaction, is derived by using the momentum transfer cross-section of HI–HII presented in Hunter & Kuryan (1977) and Draine (1980).

To compute accurate energy exchange rates, we solve the chemical equations without assuming ionization–recombination equilibrium. We consider only 6 chemical reactions, which are ionization and recombination for HI–HII, for HeI–HeII and for HeII–HeIII. This non–equilibrium approach is important behind shock fronts, where a description using the Saha equation would overestimate the ionization fraction, and would lead to wrong abundances and wrong energy exchange rates. We use the chemical reaction rates presented in Cen (1992).

In rich galaxy clusters, the gas temperature ranges from 1 to 10 keV. Line cooling is therefore negligible. We only take into account Brehmstrahlung (Mewe et al. 1987) and Compton cooling by the Cosmic Background Radiation (Peebles 1993). These cooling processes are likely to lower slightly the electrons temperature, and therefore enhance the departure from thermodynamical equilibrium.

In Teyssier et al. (1997), we also considered the influence of electronic conduction, assuming no transverse magnetic field. We showed that conduction is effective only in the very low density, outer regions, where a thermal precursor preheats the gas ahead of the shock front (Zel’dovich & Raizer 1966). The downstream flow properties were qualitatively similar to the non conductive case, although the temperature decoupling between ions and electrons was slightly lowered. This led us to conclude that, even in the assumption of no magnetic field, electronic conduction might have no direct observational consequences. On the other hand, it has been shown that a small magnetic field ($\simeq 1 \mu G$) does exist in the intracluster medium (Kim et al. 1990). Electronic conduction should then be efficiently suppressed. We therefore do not consider it in the present paper.

The presence of a magnetic field does not affect classical collisional energy exchange, since it is a purely local process. However, a magnetic field has also the well-known effect of introducing various plasma instabilities within the shock structure. These instabilities are believed to be responsible of a rapid, anomalous heating of electrons. Cargill & Papadopoulos (1988) proposed a mechanism for this strong, collisionless heating, based on the Buneman and ion acoustic instabilities. This mechanism justifies why electrons are efficiently heated in young supernovae remnants, an observational fact which was unexplained by the classical collisional theory. However, Cargill & Papadopoulos (1988) showed that only 12% of the upstream kinetic energy can be converted into electrons thermal energy. Consequently, after the collisionless shock front, complete ions-electrons equipartition still relies on classical collisional processes. In the calculations we present in this paper, although we neglect the various plasmas instabilities discussed here, we obtain rather low temperature differences, namely $T_e \geq T_i/5$. This justifies the use of classical collisions theory only.

Keeping in mind the physical assumption we just made, let us now summarize the thermodynamical history of the intracluster gas. Ions and neutrals are shock heated through mergers or accretion shock waves. Electrons are less efficiently heated by shocks, as can be shown by hand using the Rankine–Hugoniot discontinuities relations. As a matter of fact, these relations state that a gas with mean molecular weight μ is heated by a shock front with velocity D up to a post-shock temperature given by

$$kT = \frac{3}{16}\mu D^2 \quad (2)$$

in the limit of very high Mach number. Just after the compression front, electrons temperature is therefore much lower than ions temperature $T_e \simeq (m_e/m_p)T_i$, where the pre-factor on the r.h.s is of the order of 10^{-3} . The plasma finally reaches thermodynamical equilibrium ($T_e \simeq T_i$) after a few ions–electrons energy exchange time–scales t_{ei} , given by equation (1)

$$t_{ei} \simeq 503 \frac{T_e^{3/2}}{n_e} \text{ sec} \quad (3)$$

The length of this so-called “equipartition wave” where a significant departure from thermodynamical equilibrium is expected, can be estimated using $L_{ei} \simeq (1/4)t_{ei}D$. Under the rather extreme physical conditions encountered in large X-ray clusters, $n_e \simeq 10^{-5}$ and $D \simeq 1000 \text{ km s}^{-1}$, this “equipartition mean free length” is very extended, $L_{ei} \simeq 1.4 \text{ Mpc h}^{-1}$. Moreover, one clearly sees from equation (3), that the higher is the gas temperature,

and the lower is the gas density, the larger is this equipartition region. In Teyssier et al. (1997), we calculated more precisely the size of this region for a pancake of initial comoving wavelength $L = 16 \text{ Mpc h}^{-1}$, and we found $L_{ei} \simeq 1 \text{ Mpc h}^{-1}$ with a total shocked region of 2 Mpc h^{-1} .

In a fully 3D environment, shock waves interact in a very complicated pattern. Hierarchical merging means here that small, low temperature sub-structures merge together, leading to strong shocks propagating in a low density environment, especially in the outer part of X-ray clusters. Consequently, we need a 3D hydrodynamical code which self-consistently solves the gas dynamics equations with the different collisional processes previously mentioned.

2.2. Numerical Schemes

The choice of our numerical method is dictated by the specific regions of clusters we are interested in. These regions are likely to be far from thermodynamical and chemical equilibrium. First, the low value of the gas density results in rather slow collisional time-scales. Second, these regions are not relaxed, with high bulk velocities and strong shock waves, making non-equilibrium phenomena dominant. We therefore use an Eulerian hydrodynamical code (Kang et al. 1994) to simulate the formation of a large cluster of galaxies.

Our code, called HYDREL, has been presented in great details for its 1D version in Teyssier et al. (1997). We briefly recall here its main characteristics, as well as the specific 3D features. HYDREL is based on an operator splitting algorithm, and solves the different thermo- and hydrodynamical equations in 3 consecutive steps. The first step, called the gravity step, solves the Poisson equation. It calculates the gravitational potential deduced from the gas and dark matter density fields. Dark matter particles are displaced during this step with a classical Particle–Mesh (PM) scheme (Hockney & Eastwood 1981), developed by Alimi and Scholl (1993) first on Connection Machine, then implemented on Cray–YMP. The equation of motion in this PM code are solved in comoving coordinates and the Green function takes into account aliasing effects and minimizes force’s anisotropies. The time integrator of the PM has however been modified, it is now based on a predictor–corrector scheme. This allows both great accuracy and variable time–stepping which is impossible with the classical Leap–Frog scheme. The second step is the adiabatic hydrodynamical step. It solves the hydrodynamical equations using directional splitting and a staggered mesh. Shock waves are treated using the pseudo–viscosity method (Von Neumann & Richtmyer 1950). We use for that purpose a viscous tensor, and not a viscous pressure. This tensorial

formulation (Tscharnutter & Winkler 1979; Mihalas & Mihalas 1984; Stone & Norman 1992; Chièze et al. 1997) is of great importance for cosmological flows. We therefore recall now the main features of our tensorial pseudo-viscosity in 3D.

This approach relies on the assumption that dissipation in shock waves is correctly described by the Navier–Stokes equations. For each direction $i = 1, 2, 3$, we use a diagonal stress tensor, whose coordinates σ_i , are proportional to the diagonal terms of the shear tensor

$$\sigma_i = \frac{P}{c_s} \Delta x \left(\frac{\partial u_i}{\partial x_i} - \frac{1}{3} \nabla \cdot u \right) \quad (4)$$

where $\nabla \cdot u$ is the divergence of the velocity field, c_s is the local sound speed and P the thermal pressure. Non-diagonal terms in the usual Navier–Stokes stress tensor are dropped here, in order to avoid spurious turbulent effects. Indeed, in the last formula, Δx is the mesh size. For a real viscous fluid, this term has to be replaced by the mean free path l of the gas particles, which is orders of magnitude lower than the cell size. The term “pseudo-viscosity” rely on the artificial enhancement of the mean free path ($l \rightarrow \Delta x$) due to the finite resolution of the grid. The viscous stress exerts on each fluid element a net force given by

$$F_i = - \frac{\partial}{\partial x_i} \sigma_i \quad (5)$$

Note that the three components of the pseudo-viscous force differ in general. A viscous pressure, in the contrary, would have been always isotropic. Note also that in case of an homologous flow ($\sigma_i = 0$), there is no dissipation in the flow (Mihalas & Mihalas 1984). A viscous pressure would not have been able to satisfy this fundamental physical requirement. Because shock waves result in a contraction of the fluid elements they cross, the pseudo-viscous force acts only when the following criterion is full-filled

$$\frac{\partial u_i}{\partial x_i} < \frac{1}{3} \nabla \cdot u < 0 \quad (6)$$

The hydrodynamical step we describe now is divided in two sub-steps for each direction: first the gas dynamics equations are solved in a Lagrangian way, then we re-map the new flow variables from the perturbed Lagrangian grid to the fixed Eulerian one. The Lagrangian step uses a predictor–corrector time solver, which ensures second order accuracy in time. The Eulerian step uses the Van Leer (1977) advection scheme, which ensures second order accuracy in space.

The third step is called the dissipative step. It solves all collisional processes, namely chemical reactions, energy exchange between the three thermodynamical processes and cooling. Because these processes are driven by rather stiff equations, we use for each cell an individual time-stepping. This allows us to compute new energies and abundances with high accuracy without slowing down the whole simulation. Chemical reactions and the other collisional processes are strongly coupled equations. To ensure stability, we solve the system of chemical and thermodynamical equations using the “fully implicit method”. The large hydrodynamical time-step is controlled by the Courant condition, and the small sub-time-steps are controlled by the relative variations of the chemical and thermodynamical variables in each cell. In the case of strong cooling ($t_{cool} < t_{dyn}$), the pressure can be dramatically underestimated. We therefore impose that during the dissipative step, the total pressure does not vary more than 10%. This method works well in general, and allows a very good accuracy in the chemical calculations. However, for large clusters of galaxies, which are the purpose of this paper, cooling is not efficient, due to the high temperature of the intra-cluster gas ($T > 1$ keV) and the relatively low-densities that we obtain in our simulation.

2.3. Initial Conditions

We now present the initial conditions that we use to simulate a rich cluster of galaxies embedded in a CDM cosmogony. We use a comoving box size of 25 Mpc h^{-1} , with periodic boundary conditions. It would have been better to use a larger box, but we have to make a compromise between large scale power and spatial resolution. We made a choice similar to Anninos & Norman (1996), and thus we can compare directly our results to their calculations. We use 128^3 grid points, and the same number of dark matter particles. The numerical force is 50 % of the true gravitational force at a scale of roughly 1.5 cells. This gives an effective resolution of 300 kpc h^{-1} . This corresponds also to the hydrodynamical resolution, as shown by extensive tests (Teyssier et al. 1997).

We start our simulation at a redshift $z_i = 50$. The initial abundances are taken from Peebles (1993) for our chosen value $\Omega_B = 0.1$. The gas temperature is initially uniform and we use the relation $T(z_i) = (1 + z_i)^2 1.37 \times 10^{-2} \text{ K}$, which states that the gas temperature is strongly coupled to the CBR up to $z = 200$, and then evolves adiabatically up to z_i . Dark matter particles are initially uniformly distributed on the grid, and then displaced using the Zel’dovich approximation. The initial baryons density field is supposed to be equal to the initial Gaussian random density field. We impose a 3σ peak of length scale 4 Mpc h^{-1} at the center of the box, using the Hoffman–Ribak (1991) algorithm. We reach the final epoch

(defined as the epoch when the linear r.m.s. is equal to 1 at 8 Mpc h^{-1}) with approximately 350 time-steps, controlled by the Courant condition. The energy conservation, as defined by Cen (1992), was less than 0.8 % during the whole run.

3. RESULTS

The cluster we obtained at $z = 0$ have average characteristics (mass, size and temperature) similar to those observed for the Coma cluster. We define the cluster center as the cell of maximum X-ray emissivity. We then define the Virial radius r_{200} of the cluster as the radius of the sphere centered on the cluster center and containing a mean over-density $\bar{\delta} = 200$. We find in this way, $r_{200} = 1.6 \text{ Mpc h}^{-1}$. The total mass embedded in this radius is $M_{200} = 9.8 \times 10^{14} \text{ M}_{\odot} \text{ h}^{-1}$.

We plot in figure (1) the gas density, temperatures and ionization fraction along a line of sight which crosses the center of the cluster. We can define here three characteristic regions in the vicinity of the cluster:

- the cluster itself, which has recovered thermodynamical and chemical equilibrium,
- a large non-equilibrium region, where ions and electrons temperatures differ significantly,
- and finally the cold, unshocked inter-cluster medium.

Note that the accretion shock is relatively steep, and that the gas is very quickly ionized. We did not consider here any ionizing background, although it is strongly suggested by the Gunn–Peterson effect, but ionization by shock waves turned out to be efficient enough, as soon as the intracluster medium is concerned. The equipartition front, where T_e gradually reaches T_i , has a thickness of approximately 1.5 Mpc h^{-1} . This non-equilibrium region stands mainly outside the Virial radius of the cluster. The shock front, which marks the beginning of the non-equilibrium region, is located at roughly $2r_{200}$ of the cluster center. The temperature decoupling between ions and electrons is maximum just after the shock front, but always greater than $T_e \simeq T_i/3$ (except “inside” the shock front). This justifies a posteriori our assumption that plasma instabilities could be neglected here (see Section 2.1).

In figure (2), we plot gray scale images of the dark matter density contrast, the gas density contrast and the electrons and ions temperatures. Note that the filamentary structures clearly converge towards the cluster. Gas and dark matter isocontours have

similar elliptical shapes, with axis ratio 2:1. They are both relatively smooth. In the contrary, the temperatures isocontours show very complicated patterns, with several shock waves propagating in different directions. Note that the electrons temperature appears much smoother than the ions temperature. The hottest regions are not located in the center of the cluster, but in the outer regions where strong shock heating occurs. This explains why the strongest temperature decoupling is mainly located in the low density, outer regions of the cluster.

We plot in figure (3) the spherically averaged density and temperatures profiles. The radius is expressed in units of r_{200} . The most inner point corresponds to our resolution limit in the computation of the gravitational force. Note that gas and dark matter density profiles are both very similar. We show no evidence of core radii in any mass distribution. Moreover, both density profiles are well fitted by a power law $\rho \propto r^{-9/4}$. This is in good agreement with Anninos & Norman (1996), who studied the influence of numerical effects on gas and dark matter density profiles, using higher resolution simulations. The electrons and ions temperatures profiles show again clearly that a large non-equilibrium region extends from $r_{200}/2$ up to $2r_{200}$. In order to quantify the error that one observer does between the X-ray temperature T_e and the true dynamical temperature $T \simeq (T_e + T_i)/2$, we plot the ratio $(T - T_e)/T$ as a function of radius. The maximum departure from thermodynamical equilibrium is located at r_{200} and is about 20%. We also calculate the ratio between the bulk kinetic energy and the internal energy of the gas. This ratio is equal to unity at r_{200} , showing that hydrostatic equilibrium is also not recovered in this region. Therefore, the hydrostatic equilibrium assumption and the thermodynamical equilibrium assumption are both valid in the central region of the cluster ($r < r_{200}/2$), but are both violated in the outer regions of the cluster ($r > r_{200}/2$).

4. CONCLUSION

In this paper, we studied the formation of a rich X-ray cluster. We found that the total mass embedded in the Virial radius ($r_{200} = 1.6 \text{ Mpc h}^{-1}$) was equal to $10^{15} \text{ M}_\odot \text{ h}^{-1}$. We found also that the density profiles of gas and dark matter are both well fitted by a $r^{-9/4}$ power law. We therefore have similar conclusions than Anninos & Norman (1996), using similar initial conditions. We studied more specifically the thermodynamical history of the intra-cluster gas. We found that a significant decoupling between electrons and ions temperatures occurs between $r_{200}/2$ and the shock front, located roughly at $2r_{200}$. The maximum departure is found at r_{200} and reaches 20%. Therefore, the usual assumption of thermodynamical equilibrium between ions and electrons breaks down in this region.

We also checked that the hydrostatic equilibrium assumption was not valid in the outer regions of the simulated cluster. These two errors can both lead to an underestimates of the gravitational mass in the outer regions of X-ray clusters ($r \geq r_{200}/2$). These results could be carefully extrapolated to the case of A2163. As mentioned in the introduction, Markevitch et al. (1996) measured at the Virial radius of A2163 a temperature of 4 keV, which is roughly equal to twice the value we found here for our simulated cluster. This could lead to a thermodynamical decoupling of 50 %, which means that the (observed) electrons temperature underestimates by a factor of two the true dynamical temperature. Therefore, for A2163, the error in the mass estimate due to a departure from thermodynamical equilibrium could be as large as a factor of two. Further studies are however required to confirm these conclusions, using other types of initial conditions.

We would like to thank R. van den Weygaert for providing us the code which generates constrained realizations of Gaussian random fields (van den Weygaert & Bertschinger 1995).

REFERENCES

- Alimi, J.-M., & Scholl, H., 1993, *Int Journal of Mod. Phys. C*, 4, 197.
- Anninos, P.A., & Norman, M.L., 1996, *ApJ*, 459, 12.
- Arnaud, M., Hughes, J.P., Forman, W.J., Jones, C., Lachièze-Ray, M., Yamashita, K., Hatsukade, I., 1992, *ApJ*, 390, 345.
- Bardeen, J.M., Bond, J.R., Kaiser, N., & Szalay, A.S., 1986, *ApJ*, 300, 15.
- Cargill, P.J., & Papadopoulos, K., 1988, *ApJ*, 329, L29.
- Cen, R.Y., 1992, *ApJS*, 78, 341.
- Chièze, J.-P., Teyssier, R., & Alimi, J.-M., 1997, *ApJ*, in press.
- Draine, B.T., & Katz, N., 1986, *ApJ*, 306, 655.
- Draine, B.T., 1980, *ApJ*, 246, 1045.
- Evrard, A.E., Metzler, C.A. & Navarro, J.F., 1996, *ApJ*, 469, 494.
- Hockney, R.W., & Eastwood, J.W., 1981, “Computer Simulations Using Particles” (New York McGraw-Hill).
- Hoffman, Y. & Ribak, E., 1991, *ApJ*, 380, 5.

- Hunter, G., & Kuryan, M., 1977, *Proc. Roy. Soc. London*, 353, 575.
- Kang, H., Ostriker, J.P., Cen, R., Ryu, D., Hernquist, L., Evrard, A.E., Bryan, G.L., & Norman, M.L., 1994, *ApJ*, 430, 83.
- Kim, K.-T., Kronberg, P.P., Dewdney, P.E., & Landecker, T.L., 1990, *ApJ*, 355, 29.
- Mihalas, D. & Weibel Mihalas, B., 1984, “Foundations of Radiation Hydrodynamics” (Oxford University Press, New York)
- Markevitch, M., Mushotzky, R., Inoue, H, Yamashita, K, Furuzawa, A. & Tawara, Y., 1996, *ApJ*, 456, 437.
- Mewe, R., Schrijver, C.J., Lemen, J.R., & Bentley, R.D., 1986, *A&AS*, 65, 511.
- Peebles, P.J.E. 1993, “Principles of Physical Cosmology” (Princeton University Press).
- Schindler, S., & Muller, E., 1993, *A&A*, 272, 137.
- Spitzer, L., 1962, “The Physics of Fully Ionized Gases” (Interscience, New York).
- Stone, J.M., & Norman, M.L., 1992, *ApJS*, 80, 753.
- Teyssier, R., Chièze, J.-P., & Alimi, J.-M., 1997, submitted to *ApJ*.
- Tscharnuter, W.-M., & Winkler, K.-H., 1979, *Comput. Phys. Comm.*, 18, 171.
- Van de Weygaert, R. & Bertschinger, E., 1995, submitted to *MNRAS*, astro-ph/9507024.
- Van Leer, B., 1977, *J. Comput. Phys.*, 23, 276.
- Von Neumann, J., & Richtmyer, R.D., 1950, *J. Appl. Phys.*, 21, 232.
- Zel’dovich, Ya. B., & Raizer, Yu. P., 1966, “Physics of Shock Waves and High-Temperature Hydrodynamic Phenomena” (Academic Press, New York and London).

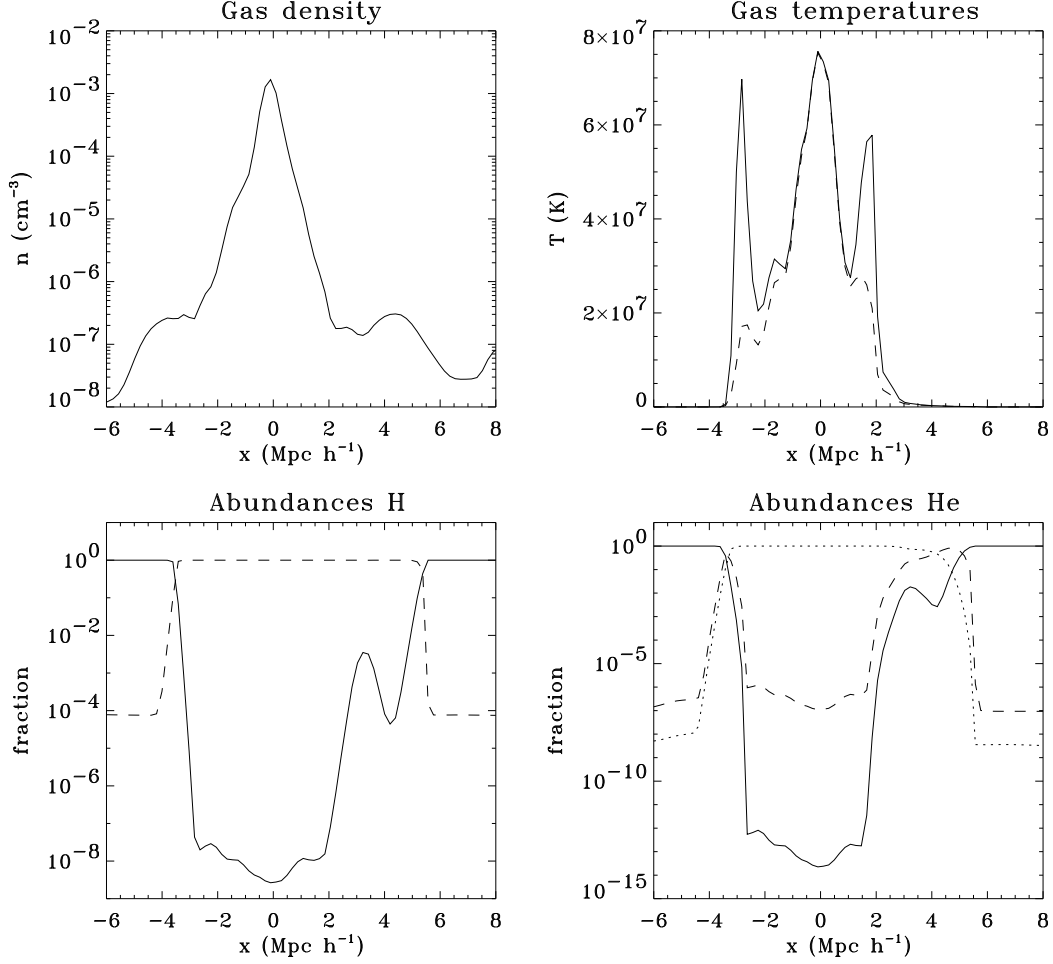


Fig. 1.— Gas density in atomic mass per cm^3 , temperatures: ions (solid line) and electrons (dashed line), abundances of Hydrogen species: fraction of HI (solid line) and HII (dashed line), abundances of Helium species: fraction of HeI (solid line), HeII (dashed line) and HeIII (dotted line). The different quantities are taken along a line of sight which crosses the cluster center.

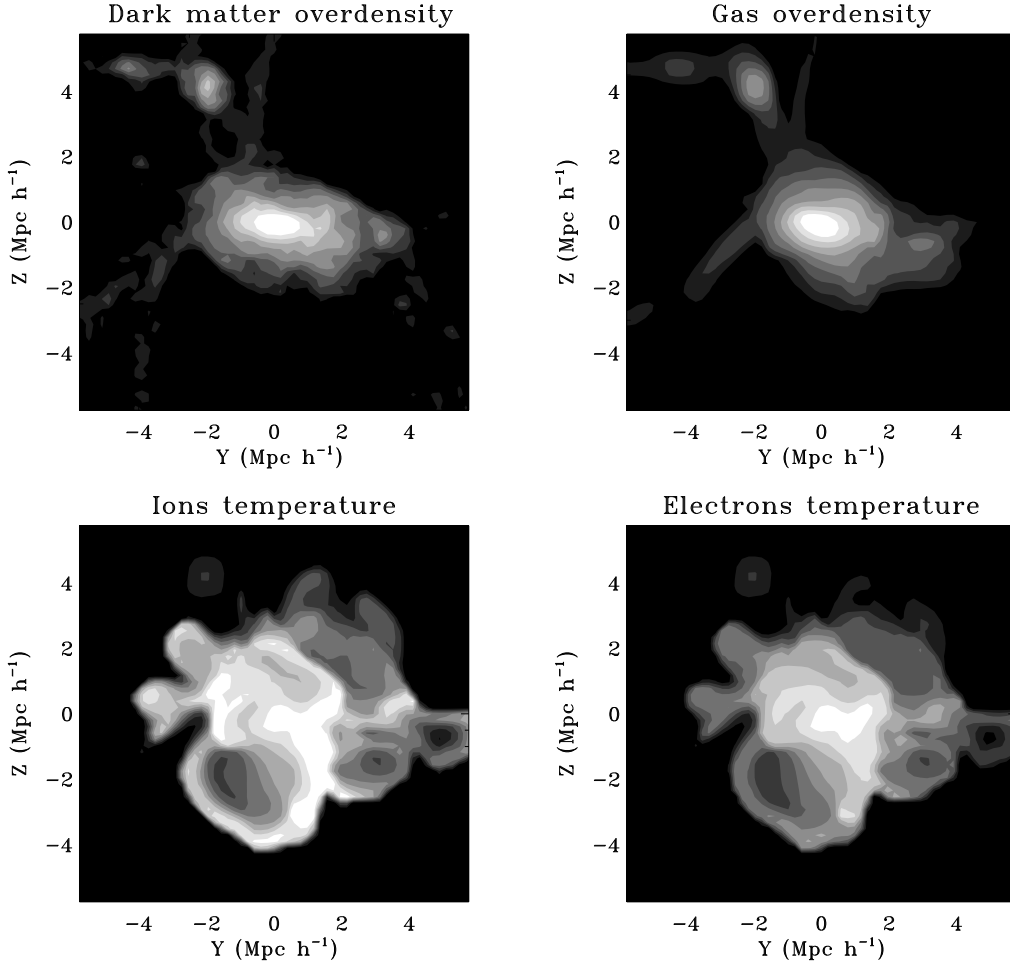


Fig. 2.— Upper panels: gray scale images of the gas and dark matter density contrast with 10 levels, defined by a constant logarithmic spacing between $\delta = 1$ and $\delta = 10^{3.5}$. Lower panels: gray scale images of the electrons and ions temperatures with 10 levels, defined by a constant logarithmic spacing between $T = 10^6$ K and $T = 10^8$ K. The slice is one-cell width and crosses the cluster center.

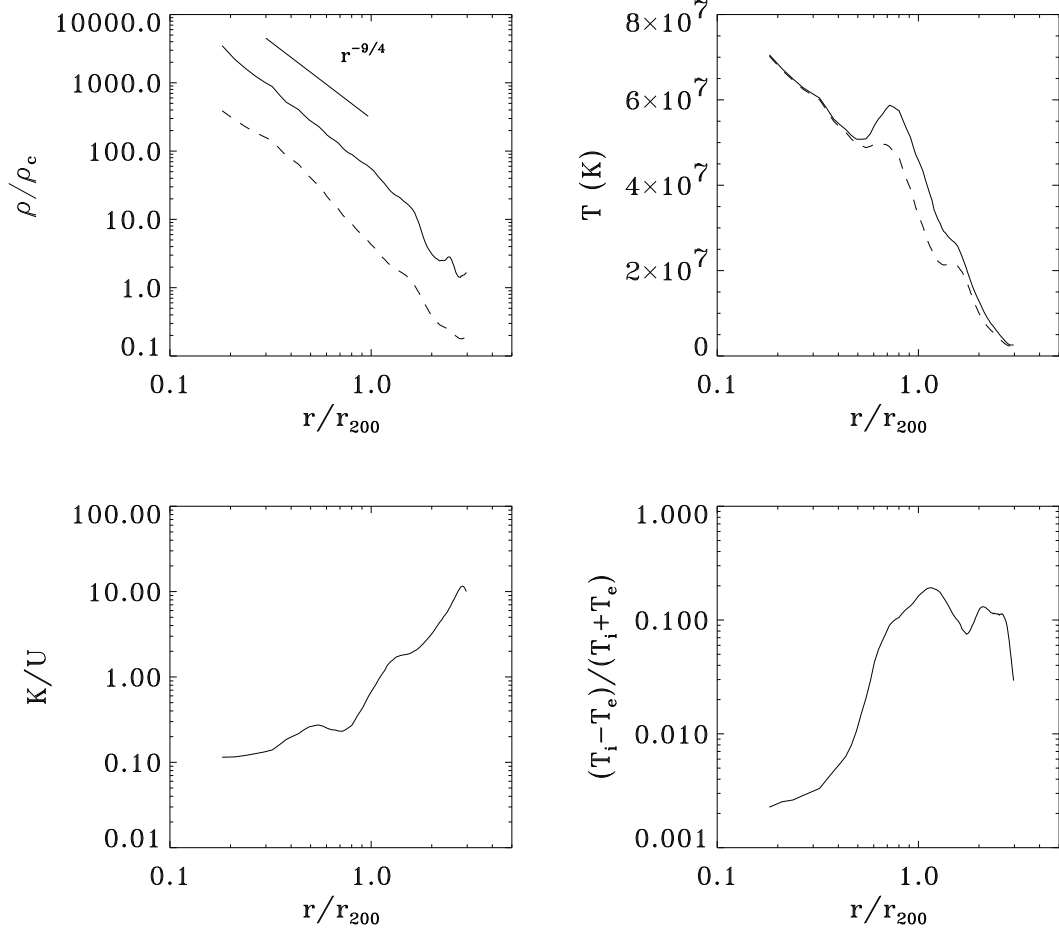


Fig. 3.— Upper left pannel: spherically averaged density profile for dark matter (solid line) and gas (dashed line) versus the radial distance to the cluster center, in units of r_{200} . The $r^{-9/4}$ power law is also shown as a straight line. Upper right pannel: spherically averaged temperature for electrons (dashed line) and ions (solid line). Lower left pannel: ratio between the bulk kinetic energy and the internal energy of the gas. Lower right pannel: ratio $(T_i - T_e)/(T_i + T_e)$ that measures the departure from thermodynamical equilibrium (see text).